Auton Robot (2008) 25: 349–365
DOI 10.1007/s10514-008-9100-0

Basic navigation, guidance and control of an Unmanned Surface Vehicle

Massimo Caccia · Marco Bibuli · Riccardo Bono · Gabriele Bruzzone

Received: 14 February 2007 / Accepted: 11 July 2008 / Published online: 6 August 2008

Abstract This paper discusses the navigation, guidance and control (NGC) system of an Unmanned Surface Vehicle (USV) through extended at sea trials carried out with the prototype autonomous catamaran Charlie. In particular, experiments demonstrate the effectiveness, both for precision and power consumption, of extended Kalman filter and simple PID guidance and control laws to perform basic control tasks such as auto-heading, auto-speed and straight line following with a USV equipped only with GPS and compass.

Keywords Autonomous vehicles · Marine robotics · Guidance systems

1 Introduction

In the last years, a growing number of Unmanned Surface Vehicles (USVs) have been developed for military, environmental and robotic research applications. In particular, as shown in Sect. 2.1, these vehicles proved their capabilities in mine countermeasures (MCM), water sampling, bathymetric survey and supporting Autonomous Underwater Vehicle (AUV) operations acting as communication relays.

In this context, the design and implementation of an accurate and reliable navigation, guidance and control system, able to operate with only linear and angular position measurements, is fundamental for the development of relatively cheap remotely controlled vehicles for civil applications. According to the approach discussed in Caccia et al. (2005), where basic automatic guidance capabilities, i.e. PD auto-heading and line-of-sight (LOS) guidance, proved to be sufficient for an unmanned catamaran to satisfactorily accomplish its operational goal, this paper demonstrates how conventional and relatively simple techniques, such as extended Kalman filters, PI gain scheduling velocity controllers, PI and PD guidance laws at the kinematic level, can enable a small unmanned catamaran to perform basic accurate manoeuvres. In particular, experiments carried out with the 2005-evolution of the Charlie prototype USV (Caccia et al. 2006), developed by CNR-ISSIA Genova, demonstrate:

1. the effectiveness of extended Kalman filter to estimate the vehicle position and speed on the basis of GPS and compass measurements and of a practical dynamic model for the prediction of the vehicle speed with respect to the water;
2. the feasibility of adopting, also for a USV equipped only with GPS and compass, a dual-loop guidance and control architecture, already satisfactorily employed on ROVs (Caccia and Veruggio 2000), where an internal loop controls the vehicle linear and angular speed and an external loop implements guidance task functions at the kinematic level;
3. the effectiveness of a simple PD guidance law in following a straight line naturally zeroing the static errors introduced by sea current disturbances, in virtue of an integrator embedded in the system kinematics.

Although a complete formal demonstration of the overall system stability lacks, the experimental demonstration of the implemented navigation, guidance and control architecture

M. Caccia (✉) · M. Bibuli · R. Bono · G. Bruzzone
CNR-ISSIA Genova, Via De Marini 6, 16149, Genova, Italy
e-mail: max@ge.issia.cnr.it

M. Bibuli
e-mail: marco@ge.issia.cnr.it

R. Bono
e-mail: riccardo.bono@ge.issia.cnr.it

G. Bruzzone
e-mail: gabry@ge.issia.cnr.it

and algorithms, mainly based on common sense considerations about the properties of the linearised system, gives a fundamental contribution in bridging the gap between theory and practice. Indeed, the relatively fast and simple development of easy manoeuvrable vessels allows the demonstration of their operational capabilities and facilitates the experimental investigation of new NGC, sensing and mission control techniques, pushing the development of marine robots that will, in the long term, afford end-users advanced tools for marine exploration and exploitation.

The paper is organised as it follows. An overview of the developed USV prototypes and of the adopted guidance and control techniques is given in Sect. 2. A *practical* model of system dynamics, as experimentally determined in Caccia et al. (2006), is presented in Sect. 3, while the model-based extended Kalman filters for heading, position and speed estimation are discussed in Sect. 4. The adopted PI gain scheduling design of angular and linear velocity controllers is reminded in Sect. 5, while Sect. 6 deals with conventional PI-type auto-heading and PD line-following technique. Experimental set-up and results are described and discussed in Sects. 7 and 8.

2 Background

2.1 Prototype USV overview

For an extended discussion of the developed prototypes and basic research issues in the field of USVs the reader can refer to Caccia (2006). Before of a brief discussion of basic design issues and trends as well as main limitations to extended civil applications, some of the most interesting prototype USVs are listed in the following:

1. the family of autonomous vessels developed at MIT for education and civil applications, consisting of the fishing trawler-like vehicle ARTEMIS, the catamarans ACES (Autonomous Coastal Exploration System) and AutoCat (Manley 1997; Manley et al. 2000), and the kayak SCOUT (Surface Craft for Oceanographic and Undersea Testing (Curcio et al. 2005)). These USVs demonstrated the feasibility of automatic heading control and DGPS-based way-point navigation, as well as the possibility of operating autonomously collecting hydrographic data. After the integration, from the point of view of human operator interface, mission planning and computer architecture, with the MIT Odyssey class AUVs, the SCOUT kayaks are supporting the development and test of distributed acoustic navigation algorithms for undersea vehicles;
2. the autonomous vessels developed in Europe such as:
   - the Measuring Dolphin, designed and developed by the University of Rostock (Germany), for high accuracy positioning and track guidance and carrying of measuring devices (e.g. depth and current) in shallow water (Majohr and Buch 2006);
   - the autonomous catamaran Delfim, developed by the DSOR lab of Lisbon IST-ISR as a communication relay for a companion AUV (Pascoal et al. 2000) in the European Union funded project ASIMOV (Advanced System Integration for Managing the coordinated operation of robotic Ocean Vehicles), and then exploited as a stand-alone unit for collecting bathymetric maps and marine data;
   - the autonomous catamaran Charlie by CNR-ISSIA Genova (Italy), originally designed, developed and exploited for the collection of sea surface microlayer (Caccia et al. 2005), and then upgraded for robotic research on autonomous vessels;
   - the autonomous catamaran ROAZ, developed under the research activity pursued on multiple autonomous robots by the Autonomous Systems Laboratory at ISEP—Institute of Engineering of Porto (Martins et al. 2006);
   - the autonomous catamaran Springer, developed by the University of Plymouth (UK), for tracing pollutants (Xu et al. 2006);
3. the unmanned surface vessels developed for military purposes such as the testbed of the SSC San Diego, based on the Bombardier SeaDoo Challenger 2000 (Ebken et al. 2005), the Israeli Stingray USV (Stingray—Unmanned Surface Vehicle), with a top speed up to 40 knots, and Protector USV (Protector—Unmanned Naval Patrol Vehicle), equipped with electro-optic sensors, radar, GPS, inertial navigation system and a stabilised 12.7 mm machine gun, and the QinetiQ Ltd shallow water influence minesweeping system (SWIMS) (Cornfield and Young 2006), employed by the Royal Navy to support MCM operations in Iraq in 2003. SWIMS basically consisted in the development of a conversion kit to transform existing Combat Support Boats, already operated by the British Royal navy, in remote controlled vessels.

The above-mentioned prototypes reveal different approaches in basic design issues and trends:

- the catamaran hull shaped vehicle, which optimises the easiness of mounting and the loading capacity of different payloads minimising movement in rough sea, is usually preferred by research developers, while, in the military field, rigid inflatable boats (RIBs) are preferred due to their diffusion as standard vessels for naval operations and their capability in carrying on larger fuel tanks;

- electrical power supply is preferred for environmental sampling applications, where the constraint of not polluting the operating area is mandatory, while, when long missions have to be performed, e.g. in the case of coastal surveillance or MCM operations, gasoline propulsion is more practical;
- the design and development of new vehicles is typical of research institutions, while the needs of low cost development and easy transfer to the end-user motivated, even in military applications, the development of *conversion kits* to transform existing vessels in remoted controlled ones;
- the goal of fully autonomous operations is the pole star of civil and research applications, while military applications see in remote controlled vessels the solution, through suitable human-computer interactions, to optimise system performances in many different mission conditions.

Common trends are the modularity and easiness of transport of USVs, since logistical constraints are usually very narrow, as well as the introduction of constructive materials such as fibre-glass in order to built robust and light hulls.

Anyway, the main limitations to an extended use of USV technology for civil applications, i.e. in areas not restricted to maritime traffic, rely in the lack of rules for the operations of autonomous vehicles at sea and of a reliable methodology for obstacle detection and avoidance. As far as legal issues are concerned the reader can refer, for instance, to the document of the Society for Underwater Technology 'Issues Concerning the Rules for the Operation for Autonomous Marine Vehicles (AMV)—A consultation paper (7 August 2006)',[1] while the first basic steps in the direction of implementing collision avoidance strategies according to the rules of the road have been presented in Benjamin and Curcio (2004). Preliminary work on automatic obstacle detection is being carried out in the military field such as in the tentative of integrating a radar and artificial vision devices on the SSC San Diego (Ebken et al. 2005). Laser-gated intensified CCD (LGICCD) could represent a dramatic improvement in obstacle detection at sea, at least during night operations, thanks to the property of the auxiliary laser light source of being completely absorbed by the water.

2.2 USV guidance and control state-of-the-art

As far as the design of basic autopilots, controlling the vehicle's heading and speed, is concerned, operational results showed that in many practical applications a simple P(I)D heading controller is sufficient for guaranteeing satisfactory performance in controlling the horizontal motion of a USV, as in the case of the sea surface microlayer sampling carried out by CNR-ISSIA Charlie (Caccia et al. 2005) and of tests performed with the SCOUT ASC (Curcio et al. 2005). Anyway, more advanced control techniques have been evaluated. For instance, a dual nested loop H_2 controller, where the inner yaw rate loop guarantees stability, robustness and disturbance rejection, and the outer position one improves follow-up performance, has been satisfactorily applied to MESSIN course control (Majohr and Buch 2006). A more general approach has been proposed in Pascoal et al. (2006), where gain-scheduling controllers, interpolating the parameters of linear controllers designed at different forward speeds, are proposed. In particular, the H_∞ performance criterion used for designing the linear controllers allows a unified treatment of control and motion estimation, performed through complementary filter techniques, in a frequency domain based approach (Fryxell et al. 1996).

In many applications, the vehicle is required to follow desired paths with great accuracy with a speed profile specified by the end-user, relaxing the strong constraints typical of trajectory tracking, defined as requiring the vessel to follow a time-parameterised reference curve, i.e. to be in specific points at specific instants of time. Thus, the so-called path following problem is faced, i.e. the vehicle has to follow a planar path without temporal constraints, usually obtaining smoother convergence to the desired path with respect to the trajectory tracking controllers, less likely pushing to saturation the control signals (Encarnaçao and Pascoal 2001). A number of path following techniques has been proposed in the literature basically originated by ideas developed for wheeled robots. Path following algorithms have to define, compute and reduce to zero the distance between the vehicle and the path as well as the angle between the vector representing the vessel speed and the tangent to the desired path. A solution based on gain-scheduling control theory and the linearisation of a generalised error vector about trimming paths has been proposed in Pascoal et al. (2006) and implemented and run on the Delfim ASC. Currently, research focuses on the development of nonlinear control design methods able to guarantee stability globally and not only locally as in the above-mentioned approach. In particular, backstepping control design methodologies and *follow-the-rabbit* path following techniques have been combined (Encarnaçao and Pascoal 2001; Lapierre et al. 2003), and a preliminary experimental validation for USVs has been presented in Bibuli et al. (2007). The role of the guidance system, computing all the reference signals needed to make the physical system autonomous, as well as the need of developing the guidance theory at the kinematic level in order to make it as general as possible, are discussed in Breivik and Fossen (2004), where a parameter adaptation technique is proposed to introduce integral action for environmental disturbance compensation. Anyway, path follower performances can be enhanced by using preview controller design techniques as introduced in Gomes et al. (2006). It is worth

[1] See http://sig.sut.org.uk/urg_uris/URG_AMV_paper.pdf.

noting that, in many practical applications, requiring the vessel roughly navigating through a sequence of way-points, conventional line-of-sight guidance, based on directing the vehicle prow towards the goal at each time, provides satisfactorily performance, in particular, from the point of view of motion smoothness and actuator activity.

3 Modelling

Assuming that the vessel motion is restricted to the horizontal plane, i.e. neglecting pitch, roll and heave, two reference frames are considered: an inertial, earth-fixed frame $\langle e \rangle$, where position and orientation $[x\ y\ \psi]$ of the vessel are usually expressed, and a body-fixed frame $\langle b \rangle$, where surge and sway velocities ($[u\ v]$ absolute, $[u_r\ v_r]$ with respect to the water), yaw rate r, and force and moments $[X\ Y\ N]$, are represented. See Fig. 1 for a pictorial representation of the Charlie USV, including reference frames, absolute and relative speed, actuator location and rudder angles.

Denoting with $[\dot{x}_C\ \dot{y}_C]^T$ the sea current, the body-fixed absolute velocity and velocity with respect to the water are related by

$$\begin{aligned} u &= u_r + \dot{x}_C \cos\psi + \dot{y}_C \sin\psi \\ v &= v_r - \dot{x}_C \sin\psi + \dot{y}_C \cos\psi \end{aligned} \tag{1}$$

and the vehicle kinematics is usually expressed in the earth-fixed frame $\langle e \rangle$ as

$$\begin{aligned} \dot{x} &= u_r \cos\psi - v_r \sin\psi + \dot{x}_C \\ \dot{y} &= u_r \sin\psi + v_r \cos\psi + \dot{y}_C \\ \dot{\psi} &= r \end{aligned} \tag{2}$$

relating vehicle speed in the earth-fixed and body-fixed frames.

As far as dynamics is concerned, a *practical* model for a small catamaran has been defined in Caccia et al. (2006), where *practical* basically stands for consistent, from the point of view of the degree of accuracy, with the quality in terms of noise and sampling rate of the measurements provided by the sensors available onboard the testbed USV, i.e. GPS and compass only. In particular, a set of steady-state and zig-zag manoeuvres have been performed with the prototype USV Charlie, while collecting data with the on-board compass and GPS, in order to identify the vehicle drag and inertia parameters. A general theoretical model of the vehicle hydrodynamics has been considered and simplifications have been performed on the basis of reasonable assumptions and the consistency and quality of the parameter estimates. For the small prototype catamaran used for the experiments, the result is that, since it was not possible to determine the sway speed with respect to the water as well as the coupling terms between surge and yaw equations with the available

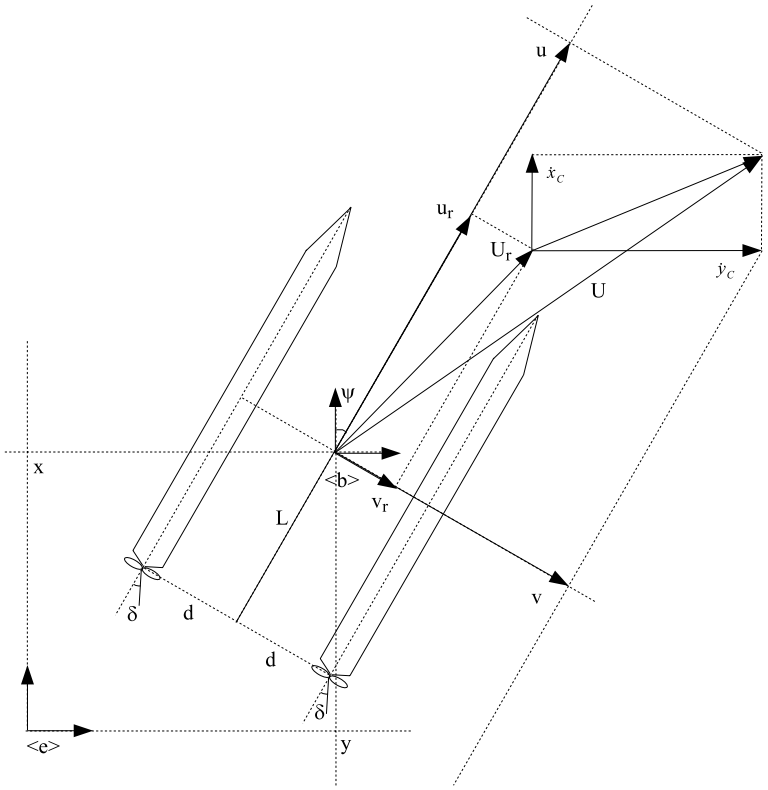

Fig. 1 Charlie USV basic nomenclature

measurements, they have been neglected and the dynamics reduced to

$$\tilde{m}_u \dot{u}_r = \tilde{k}_u u_r + \tilde{k}_{u_r^2} u_r^2 + \tilde{k}_{\bar{n}^2\delta^2} \bar{n}^2 \delta^2 + \bar{n}^2 \tag{3}$$

$$\tilde{I}_r \dot{r} = \tilde{k}_r r + \tilde{k}_{r|r|} r|r| + \tilde{k}_{\bar{n}^2} \bar{n}^2 + \bar{n}^2 \delta \tag{4}$$

where δ is the rudder angle, $\tilde{m}_u$ and $\tilde{I}_r$ are the inertia terms, $\tilde{k}_u$, $\tilde{k}_{u_r^2}$, $\tilde{k}_r$ and $\tilde{k}_{r|r|}$ are the drag coefficients. Since in the case the vessel is equipped with servo-amplifiers closing a hardware thruster revolution rate control loop with time constant negligible with respect to the system, the propeller revolution rate n is proportional to the reference voltage V applied by the vehicle control system. Thus, a normalised propeller revolution rate $\bar{n}$, expressed in Volts, and proportional to n due to the action of the servo-amplifiers, is used in the model. It is worth noting that, at steady-state, the vessel speed u resulted to be about proportional to the normalised propeller revolution rate $\bar{n}$, making the dependency of the rudder drag and torque from the surge speed not observable with respect to the available sensors. Thus, $\tilde{k}_{\bar{n}^2\delta^2}$ represents the resistance due to the rudder, and $\tilde{k}_{\bar{n}^2}$ takes into account the vessel longitudinal asymmetries, which change with the different payload configurations. This term is included in the identification model, and is usually neglected, i.e. assumed equal to zero and compensated by the control action, when designing the control laws.

Since in (4), the steering torque $\bar{n}^2\delta$ has been identified as function of the propeller revolution rate instead of the advance speed, the rudder action is neglected when the vehicle is still moving while $\bar{n}$ is zero. Thus, the field of validity of the proposed model of vehicle dynamics is for $\bar{n} > \bar{n}_{min} > 0$ and when the actual speed of the vehicle follows closely the temporal evolution of $\bar{n}$.

4 Motion estimation

The vehicle motion is estimated on the basis of measurements of heading and linear position and of the reference rudder angle and normalised propeller revolution rate only. Anyway, although simplified, a model of the surge and yaw dynamics of the vehicle is available and can be used as a kind of virtual sensor for yaw and surge derivative measurements in order to increase the filter performance in terms of smoothness and delay of the estimates. This practical approach has already proved its effectiveness, for instance, in the estimate of the heave motion of an ROV when only quite noisy depth measurements are available (Caccia and Veruggio 1999).

As far as yaw motion is concerned, the heading measurements $\psi_m = \psi + \xi_\psi$ are provided by the vehicle compass (ξ_ψ represents the measurement noise). Since the vessel longitudinal asymmetries change with the payload configuration, the system state $[\psi\ r\ \tilde{k}_{\bar{n}^2}]^T$ includes also the parameter $\tilde{k}_{\bar{n}^2}$ in addition to the vehicle heading ψ and yaw rate r, and the system equations are given by:

$$\begin{aligned}
\dot{\psi} &= r \\
\dot{r} &= \frac{\tilde{k}_r}{\tilde{I}_r} r + \frac{\tilde{k}_{r|r|}}{\tilde{I}_r} r|r| + \frac{\bar{n}^2}{\tilde{I}_r} \tilde{k}_{\bar{n}^2} + \frac{1}{\tilde{I}_r} \bar{n}^2 \delta + \xi_{\bar{n}^2\delta} \\
\dot{\tilde{k}}_{\bar{n}^2} &= \xi_{k_{\bar{n}^2}}
\end{aligned} \tag{5}$$

where $\xi_{\bar{n}^2\delta}$ and $\xi_{k_{\bar{n}^2}}$ represent system noise. The state is then estimated by a conventional extended Kalman filter (EKF), which gives an approximation of the optimal estimate (see, for instance, Ribeiro 2004 for EKF discussion and details).

On the other hand, the vehicle linear motion is described by the following equations

$$\begin{aligned}
\dot{x} &= \left(u_r + \xi_{u_r}\right) \cos\psi + \dot{x}_C \\
\dot{y} &= \left(u_r + \xi_{u_r}\right) \sin\psi + \dot{y}_C \\
\ddot{x}_C &= \xi_{\dot{x}_C} \\
\ddot{y}_C &= \xi_{\dot{y}_C}
\end{aligned} \tag{6}$$

where ξ_{u_r}, $\xi_{\dot{x}_C}$ and $\xi_{\dot{y}_C}$ model the system noise errors in surge estimate and the slow sea current variations.

It is clear that, when only position and heading measurements are available, it is not possible to discriminate between the vehicle speed with respect to the water and the sea current, thus having the possibility of estimating only the vessel absolute speed. Anyway, the open-loop integration of (3) can provide an estimate of the vehicle surge with respect to the water. In spite of the errors due to the always present mismatches between nominal and actual vehicle parameters, this estimate of the vehicle surge proved its usefulness in reducing the delay and increasing the smoothness in the linear motion estimates. The result is that the vehicle surge speed with respect to the water u_r is estimated on the basis of the normalised propeller revolution rate and rudder deflection by online integrating (3), i.e. implementing a kind of virtual velocity sensor consisting of an open-loop model-based predictor in the manner presented in Caccia and Veruggio (1999). Once the vehicle heading and surge are estimated by the yaw motion EKF and the virtual speed sensor respectively, assumed the system state as $[x\ y\ \dot{x}_C\ \dot{y}_C]^T$ and the state equations given by (6), the linear motion of the vehicle, given the GPS measurements of its position, can be estimated by conventional complementary (Fryxell et al. 1996) or Kalman filter.

In this case, a linear time-varying Kalman filter has been implemented with the following trick to compensate for the discontinuities of the GPS signal described in Caccia et al. (2006). The system state has been augmented with the vector $\underline{\hat{x}}_{offset} = [x_{offset}\ y_{offset}]^T$ representing a piecewise constant

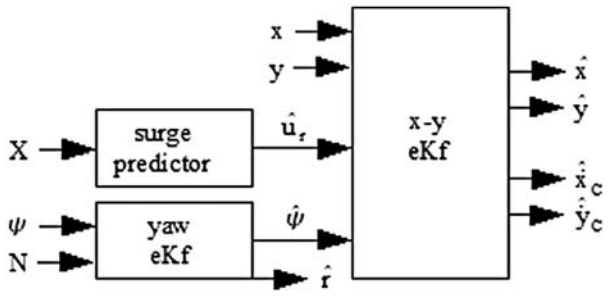

Fig. 2 Motion estimation system architecture

measurement disturbance

$$x_{offset}(t) = \sum_{i=1}^{k} \partial x_k S(t - t_k)$$

$$y_{offset}(t) = \sum_{i=1}^{k} \partial y_k S(t - t_k)$$

where $S(\tau)$ is the step function, i.e. $S(\tau) = 0, \tau < 0$ and $S(\tau) = 1, \tau \geq 1$, and ∂x_k and ∂y_k represent the disturbance step amplitudes. Thus, the measurement equations are

$$\begin{aligned} x_m &= x + x_{offset} + \eta_x \\ y_m &= y + y_{offset} + \eta_y \end{aligned} \tag{7}$$

where $[\eta_x \ \eta_y]^T$ represent the GPS measurement noise.

When a new position measurement $\underline{x}_m(k)$ is available at step k, its distance from its expected value $\underline{\hat{x}}_m(k/k-1) = \underline{\hat{x}}(k/k-1) + \hat{x}_{offset}(k/k-1)$ is checked in order to evaluate if a discontinuity in the position measurement occurs. In particular, the following inequality is considered:

$$\left(\underline{x}_m - \underline{\hat{x}}_m\right)^T \left(P_{xy} + P_{\eta_{xy}}\right)^{-1} \left(\underline{x}_m - \underline{\hat{x}}_m\right) \leq \lambda \tag{8}$$

where P_{xy} and $P_{\eta_{xy}}$ represent the covariance of the vehicle position estimate and of measurement noise respectively, and the indices of the referred steps have been omitted for the sake of compactness.

In the case inequality (8) does not hold, the Kalman filter performs a pure prediction step and the measurement offset is updated according to $\underline{\hat{x}}_{offset}(k/k) = \underline{x}_m(k) - \underline{\hat{x}}(k/k)$ and $\underline{\hat{x}}_{offset}(k+1/k) = \underline{\hat{x}}_{offset}(k/k)$.

The resulting motion estimation system, constituted by a couple of Kalman filters for yaw and linear motion respectively and a surge predictor, is shown in Fig. 2, where X and N represent the normalised control force $\bar{n}^2$ and torque $\bar{n}^2\delta$ respectively. The absolute vehicle speed in the earth-fixed frame $\langle e \rangle$ is computed on the basis of (1).

5 Control

In order to design linear and angular velocity controllers, a simplified version of the model given by (1), (3) and (4) has been considered, neglecting, i.e. considering as external disturbances, the resistance due to the rudder and the vessel longitudinal asymmetries as well as the sea current. The result is the following generic 1-dof model for surge and yaw motion:

$$\tilde{m}_\xi \dot{\xi} = \tilde{k}_\xi \xi + \tilde{k}_{\xi|\xi|} \xi |\xi| + \tau \tag{9}$$

where $\tilde{m}_\xi$, $\tilde{k}_\xi$ and $\tilde{k}_{\xi|\xi|}$, Ξ represent inertia and drag coefficients and control action respectively.

On this basis, a PI gain scheduling controller of the type already used for the control of remotely operated vehicles (Caccia and Veruggio 2000) can be adopted. Controller design and properties are summarised in the following for the sake of completeness.

Consider the generic nonlinear system

$$\tilde{m}_\xi \dot{\xi} = f(\xi) + \tau \tag{10}$$

and a conventional PI feedback scheme, where ϕ represents the reference value. Linearization of (10) about the operating point $\xi = \phi = \alpha$ and $\tau = \tau(\alpha) : \dot{\xi}[\alpha, \tau(\alpha)] = 0$, i.e. $\tau(\alpha) = -f(\alpha)$, results in the family of parameterized linear models

$$\dot{\xi}_\delta = \frac{f'(\alpha)}{\tilde{m}_\xi} \xi_\delta + \frac{1}{\tilde{m}_\xi} \tau_\delta \tag{11}$$

where $\xi_\delta = \xi - \alpha$ and $\tau_\delta = \tau - \tau(\alpha)$.

Thus, according to Khalil (1996), it is possible to design a parameterised family of PI linear controllers at each constant operating point α

$$\tau_\delta = k_P e + k_I \gamma \qquad \dot{\gamma} = e = \xi - \phi = \xi_\delta - \phi_\delta \tag{12}$$

where $\phi_\delta = \phi - \alpha$.

In order to obtain a desired characteristic equation for the closed-loop linearized system of the form

$$s^2 + 2\sigma s + \sigma^2 + \omega_n^2 = 0 \quad \sigma > 0 \tag{13}$$

the gains $k_P(\alpha) = -f'(\alpha) - 2\tilde{m}_\xi \sigma$ and $k_I = -\tilde{m}_\xi(\sigma^2 + \omega_n^2)$ are obtained.

Then, feed-forwarding the nominal steady-state control input, the controller assumes the form (see Fig. 3)

$$\tau = \tau(\alpha) + \tau_\delta \tag{14}$$

In this way, at steady-state, the integral action is completely devoted to compensate external disturbance and parametric uncertainty.

When the control given by (14) and (12) is applied to the nonlinear state (10), it results in the closed-loop system:

$$\begin{cases} \tilde{m}_\xi \dot{\xi} = f(\xi) - f(\phi) + k_P(\xi - \phi) + k_I \gamma \\ \dot{\gamma} = \xi - \phi \\ \phi = \xi \end{cases} \tag{15}$$

Fig. 3 Velocity control scheme

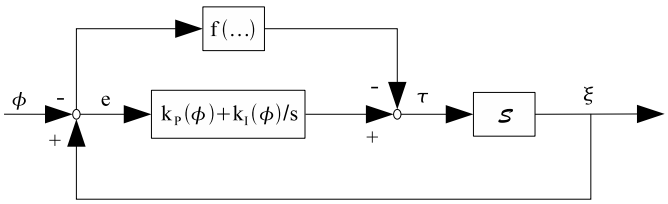

Linearization of the closed-loop system about $(\xi, \gamma) = (0, 0)$ and $\phi = \alpha$ results in the linearized closed-loop equation

$$\begin{cases} \tilde{m}_\xi \dot{\xi}_\delta = \left[f'(\alpha) + k_P(\alpha)\right]\xi_\delta + k_I \gamma \\ \qquad\qquad - \left[f'(\alpha) + k_P(\alpha)\right]\phi_\delta \\ \dot{\gamma} = \xi_\delta - \phi_\delta \end{cases} \tag{16}$$

Substituting the computed value of $k_P(\alpha) = -f'(\alpha) - 2\tilde{m}_\xi \sigma$ and $k_I = -\tilde{m}_\xi(\sigma^2 + \omega_n^2)$, the closed-loop transfer function from the command input to the output is given by

$$\frac{2\sigma s + \sigma^2 + \omega_n^2}{s^2 + 2\sigma s + \sigma^2 + \omega_n^2} \tag{17}$$

It is worth noting that the closed-loop transfer function (17) is independent by the scheduling variable ϕ.

In operating conditions an anti-windup mechanism is implemented such that $|\gamma| \leq \eta_{MAX}$.

It is worth noting that the computed normalised control actions, i.e. surge force $X = n^2$ and yaw torque $N = n^2\delta$, are mapped onto the reference propeller revolution rate and rudder angle according to the formula $\delta = \frac{N}{X}$ and $n = \sqrt{X}$.

6 Guidance

In the proposed nested dual-loop control architecture, the guidance module performs position control at the kinematic level generating suitable velocity references according to the desired task. According to this scheme, it is up to the dynamics controllers to ensure that the actual rotational and linear speed of the vehicle track the references with sufficient precision to guarantee the overall stability of the system. Although a rigorous demonstration of system stability is not given and has to be the object of further investigations, the design of guidance task functions at the kinematic level is usually very simple as well as the tuning of the kinematic and dynamic controller parameters on the basis of empirical considerations as discussed in Caccia (2007).

6.1 Heading control

As shown in Caccia and Veruggio (2000), heading control can be easily performed defining a task function of PI-type

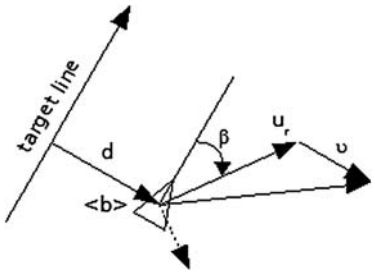

Fig. 4 Line-following nomenclature

$e = (\psi - \psi^*) + \mu \int_0^t (\psi - \psi^*)\, d\tau$. After some simple computations, the heading controller assumes the form

$$r^* = -\Gamma_P \left(\psi - \psi^*\right) - \Gamma_I \int_0^t \left(\psi - \psi^*\right) d\tau \tag{18}$$

with $\Gamma_P = \lambda + \mu$ and $\Gamma_I = \lambda\mu$, $\lambda > 0$ and $\mu \geq 0$.

In order to minimize wind-up effects, the integrator is enabled/disabled with an hysteresis mechanism when the error e gets lower/higher than I_e^{ON}/I_e^{OFF} respectively. In addition, the proportional and integral control actions are saturated so that $|\Gamma_P(\psi - \psi^*)| \leq \xi_P^{MAX}$ and $|\Gamma_I \int_0^t (\psi - \psi^*) d\tau| \leq \xi_I^{MAX}$ respectively.

6.2 Line-following

The task of steering the vessel to follow a straight line in the desired versus given the vehicle surge speed with respect to the water, $u_r > 0$, is addressed. In other words, the guidance goal is to zero the range d from the vessel and the target line, while maintaining the angle $\beta = \psi - \gamma_L$ between the desired line orientation γ_L and the vehicle heading ψ in $(-\frac{\pi}{2}, \frac{\pi}{2})$ (see Fig. 4 for line-following notation and nomenclature).

Thus, since the small prototype catamaran considered in this paper can be modelled, from the kinematics point of view, neglecting the sway speed with respect to the water (Caccia et al. 2006), denoting with υ the sea current in the direction orthogonal to the target line, the following state equations hold:

$$\dot{d} = u_r \sin\beta + \upsilon \simeq u_r \beta + \upsilon \tag{19}$$

$$\ddot{d} = u_r \dot{\beta} \cos\beta \simeq u_r \dot{\beta} \tag{20}$$

$$\dot{\upsilon} = 0 \tag{21}$$

$$\dot{\beta} = r \tag{22}$$

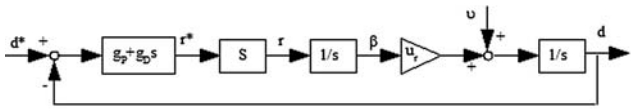

Fig. 5 Line-following guidance system: linear approximation

where the symbol $\simeq$ denotes the linear approximation for small values of β. It is worth noting that the error by approximating $\sin\beta$ with β is lower than 1% for $|\beta| \leq 14$ degrees. As shown by the block diagram of Fig. 5, considering a generic zero-error stable dynamics for the yaw rate control loop, e.g. $\frac{S_N(s)}{S_D(s)}$ with

$$S_N(s) = \sum_{i=0}^{1} p_i s^i, \qquad S_D(s) = \sum_{i=0}^{2} q_i s^i,$$

$$p_0(0) = q_0(0) \neq 0,$$

and assuming a PD guidance law for computing the desired yaw rate

$$r^* = g_P\left(d^* - d\right) - g_D\dot{d}, \quad g_P > 0,\ g_D > 0 \tag{23}$$

the transfer function for the linearised system gets

$$D(s) = \frac{u_r(g_P + g_D s)S_N(s)}{s^2 S_D(s) + (g_P + g_D s)S_N(s)} D^*(s) + \frac{s S_D(s)}{s^2 S_D(s) + (g_P + g_D s)S_N(s)} \Upsilon(s) \tag{24}$$

Equation (24) shows that, for the linearised system, i.e. for small values of β, in virtue of the integrator between r and β itself, a PD guidance law zeroes the static error introduced by sea current disturbances. It is worth pointing out that this condition can be violated in the presence of currents with speed comparable to that of the vehicle with respect to the water.

Considering the exact nonlinear expression of $\dot{d}$ given by (19), (23) gets:

$$r^* = g_P\left(d^* - d\right) - g_D\left(u_r \sin\beta + \upsilon\right) \tag{25}$$

where d^* is assumed equal to zero.

Observing the proportional part of (25) it is clear that, for large values of d, the vehicle starts to rotate around itself.

This problem can be heuristically faced by observing that the vehicle can stop to rotate around itself if

$$r^*(d,\beta) = 0 \quad \Leftrightarrow \quad \sin(\beta) = -\left(\frac{g_P}{g_D u_r} d + \frac{\upsilon}{u_r}\right), \quad \beta \in \left(-\frac{\pi}{2}, \frac{\pi}{2}\right) \tag{26}$$

Equation (26) admits a solution if and only if

$$\exists \bar{\beta} \in \left(-\frac{\pi}{2}, \frac{\pi}{2}\right) : \left|\frac{g_P}{g_D u_r} d + \frac{\upsilon}{u_r}\right| < \bar{b} = \sin\bar{\beta} \tag{27}$$

Denoting with $\bar{\upsilon}$ the maximum absolute value of the sea current υ, and remebering the positivity of g_P, g_D and u_r, (27) admits a solution if

$$|d| < \frac{g_D}{g_P}\left(u_r\bar{b} - \bar{\upsilon}\right) = \bar{d} \tag{28}$$

which, since $|d| > 0$ and $\bar{b} < 1$, embeds the trivial condition $\bar{\upsilon} < u_r$. Thus, bounding the value of d in (23), the following heuristic guidance law is obtained

$$r^* = -g_P \mathrm{sat}\left(d, -\bar{d}, \bar{d}\right) - g_D\dot{d} \tag{29}$$

which forces the vessel to approach the target line for large values of $|d|$ with β such that $r^*(\beta) = 0$, i.e. $\beta = a\sin(-\bar{b} + \frac{\bar{\upsilon}-\upsilon}{u_r})$, if $d > \bar{d}$, or $\beta = a\sin(\bar{b} - \frac{\bar{\upsilon}+\upsilon}{u_r})$, if $d < \bar{d}$, maintaining $\beta \in (-\frac{\pi}{2}, \frac{\pi}{2})$ also in the presence of the effects of measurement noise and underlying system dynamics.

It is worth noting that for large values of $|d|$ applying the control law (29) is equivalent to require a constant value of $\dot{d}$.

For instance, in the case of $d > \bar{d} > 0$, let us require $\dot{d} = \dot{d}^* = -\frac{g_P}{g_D}\bar{d}$. Noticing that the negative reference value of $\dot{d}$ implies a reduction of the value of d, consider the Lyapunov function $V_{\dot{d}} = \frac{1}{2}(\dot{d} - \dot{d}^*)$. After some computations, it is possible to verify that, when choosing $r = -g_P\bar{d} - g_D\dot{d}$ according to (29), $V_{\dot{d}} = -u_r\cos\beta(\frac{g_P}{\sqrt{g_D}}\bar{d} + \sqrt{g_D}\dot{d})^2$ which is negative definite for $\beta \in (-\frac{\pi}{2}, \frac{\pi}{2})$.

In the case, the vessel is oriented such that $\beta \notin (-\frac{\pi}{2}, \frac{\pi}{2})$, it is forced to rotate in the versus which minimises the way to the $\bar{\beta}$ orientation.

Thus, the resulting line-following guidance law is constituted by three control modes:

(a) if $\beta \notin (-\frac{\pi}{2}, \frac{\pi}{2})$ the vehicle rotates at constant yaw rate towards the $\bar{\beta}$ orientation;
(b) if $|d| > \bar{d}$ the vehicle approaches the desired straight line at constant $\dot{d}$;
(c) if $|d| \leq \bar{d}$ the vehicle follows the line with a PD guidance law.

It is worth noting that the gains g_P and g_D of (23) can be chosen such that the closed-loop system, with ideal dynamics, given by (24) has the desired characteristic equation $s^2 + 2\sigma_{LF}s + \sigma_{LF}^2 + \omega_{LF}^2$. For a surge speed with respect to the water $u_r > 0$, this means to assume

$$g_D = \frac{2\sigma_{LF}}{u_r}; \qquad g_P = \frac{\sigma_{LF}^2 + \omega_{LF}^2}{u_r} \tag{30}$$

7 Experimental set-up

Experiments have been carried out in restricted waters inside the Genova harbour with Charlie (see Fig. 6), a small autonomous catamaran prototype which is 2.40 m long, 1.70 m

Fig. 6 Charlie USV

wide and weighs about 300 Kg in air. The vessel, designed and developed by CNR-ISSIA Genova for sampling sea surface microlayer and collecting data on the air-sea interface in Antarctica (Caccia et al. 2005), is propelled by two DC thrusters whose revolution rate is controlled by a couple of servo-amplifiers, closing a hardware thruster revolution rate control loop with time constant negligible with respect to the system. With respect to the original model, the 2005-evolution of the vehicle has been upgraded with a rudder-based steering system, constituted by two rigidly connected rudders, positioned behind the propellers, and actuated by a Faulhaber 3564K024B-K1155 brushless motor with a reduction ratio of 415:1. The vessel navigation package is constituted by a GPS Ashtech GG24C integrated with a KVH Azimuth Gyrotrac, able to compute the True North given the measured Magnetic North and the GPS-supplied geographic coordinates. Electrical power supply is provided by four 12 V @ 40 Ah lead batteries integrated with four 32 W triple junction flexible solar panels.

The embedded real-time control system, developed in C++, is fully based on standard GNU/Linux as discussed in Bruzzone and Caccia (2005) and run on commercial-off-the-shelf hardware, i.e. Single Board Computer supporting serial and Ethernet communications and PC-104 modules providing digital and analog I/O.

8 Experimental results

Experiments have been carried out considering the vehicle dynamics model given by (3) and (4) with the values of the coefficients reported in Table 1, i.e. considering quadratic surge and yaw drag and neglecting the longitudinal asymmetry of the vehicle ($\tilde{k}_{n^2} = 0$). It is worth noting that the normalised propeller revolution rate $\bar{n}$ is expressed in Volts (it is the reference voltage applied to the servo-amplifiers controlling the thruster speed) and that all the coefficients have been normalised, thus changing their original measurement units.

Table 1 Charlie USV dynamics model coefficients

Surge		Yaw	
$\tilde{m}_u$	150.00 $\frac{\mathrm{V^2 s^2}}{\mathrm{m}}$	$\tilde{I}_r$	163.30 $\mathrm{V^2 s^2}$
$\tilde{k}_u$	0.00 $\frac{\mathrm{V^2 s}}{\mathrm{m}}$	$\tilde{k}_r$	0.00 $\mathrm{V^2 s}$
$\tilde{k}_{u_r^2}$	−28.48 $\frac{\mathrm{V^2 s^2}}{\mathrm{m^2}}$	$\tilde{k}_{r\|r\|}$	−703.00 $\frac{\mathrm{V^2 s^2}}{\mathrm{rad}}$
$\tilde{k}_{n^2\delta^2}$	−3.40 $\frac{1}{\mathrm{rad^2}}$	$\tilde{k}_{n^2}$	0.00 rad

As discussed in Caccia et al. (2006), the KVH Azimuth Gyrotrac provides heading measurements at 2 Hz with a standard deviation of 0.1 degrees and a maximum error of 2 degrees, while the GPS Ashtech GG24C generates piecewise continuous latitude and longitude signals at the sampling frequency of 1 Hz. Once signal discontuinuities are compensated in post-processing, the signal standard deviation is 0.17 m with a maximum error lower than 0.6 m along each component of the vehicle earth-fixed position.

8.1 Motion estimation

As far as motion estimation is concerned, the extended Kalman filter based on (5) for yaw motion estimation has been applied assuming the values $\mathrm{cov}(\xi_{n^2\delta}) = (0.2(\frac{\mathrm{deg}}{\mathrm{s}}))^2$, $\mathrm{cov}(\xi_{k_{n^2}}) = (0.0001\ \mathrm{rad})^2$ and $\mathrm{cov}(\xi_\psi) = (0.1\ \mathrm{deg})^2$ for system and measurement noise respectively.

An example of practical results, while the USV was manoeuvring with a normalised thrust of 25 V^2, is given in Fig. 7, where the measured and estimated heading are plotted, together with the estimated yaw rate and commanded rudder angle. It is worth noting that the adoption of model-based filtering techniques allows a very smooth estimate of the heading first derivative (the maximum estimate noise is lower of 0.5 deg/s) even in presence of measurements of angular position only, reducing power consumption and system wear induced by estimate noise (Caccia et al. 2003). Linear motion is estimated with an extended Kalman filter based on state and measurement (6) and (7), assuming the values $\mathrm{cov}(\xi_{u_r}) = (0.3\ \mathrm{m/s})^2$, $\mathrm{cov}(\xi_{\dot{x}_C}) = \mathrm{cov}(\xi_{\dot{y}_C}) = (0.001\ \mathrm{m/s^2})^2$ and $\mathrm{cov}(\eta_x) = \mathrm{cov}(\eta_y) = (0.17\ \mathrm{m})^2$.

Typical results are shown in Figs. 8 and 9, where the filter capability of detecting and compensating GPS measurement discontinuities is pointed out, together with the smoothness of the estimated linear speed, characterised by an estimate noise lower than 0.01 m/s.

8.2 Control

Surge and yaw rate controllers have been designed according to the PI gain-scheduling approach presented in Sect. 5,

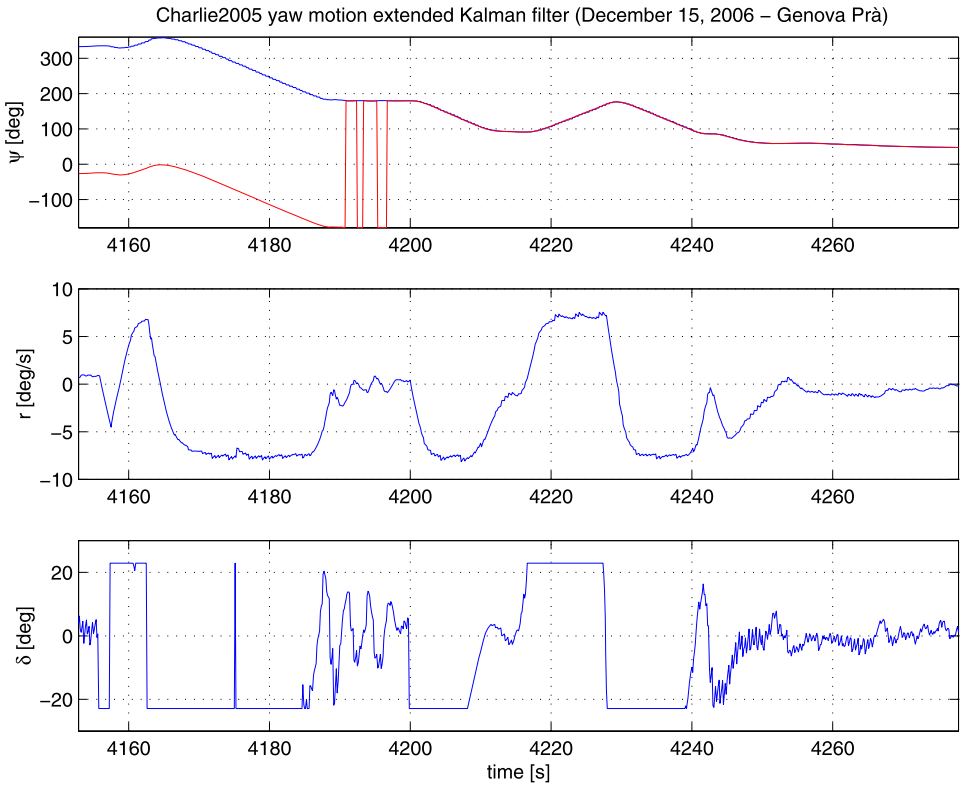

Fig. 7 (Color online) Yaw motion estimation: extended Kalman filter. From *top* to *bottom*: measured (*blue*) and estimated (*red*) heading; estimated yaw rate; reference rudder angle. The heading is measured in the range $[0, 360)$ and estimated in the range $(-180, 180]$

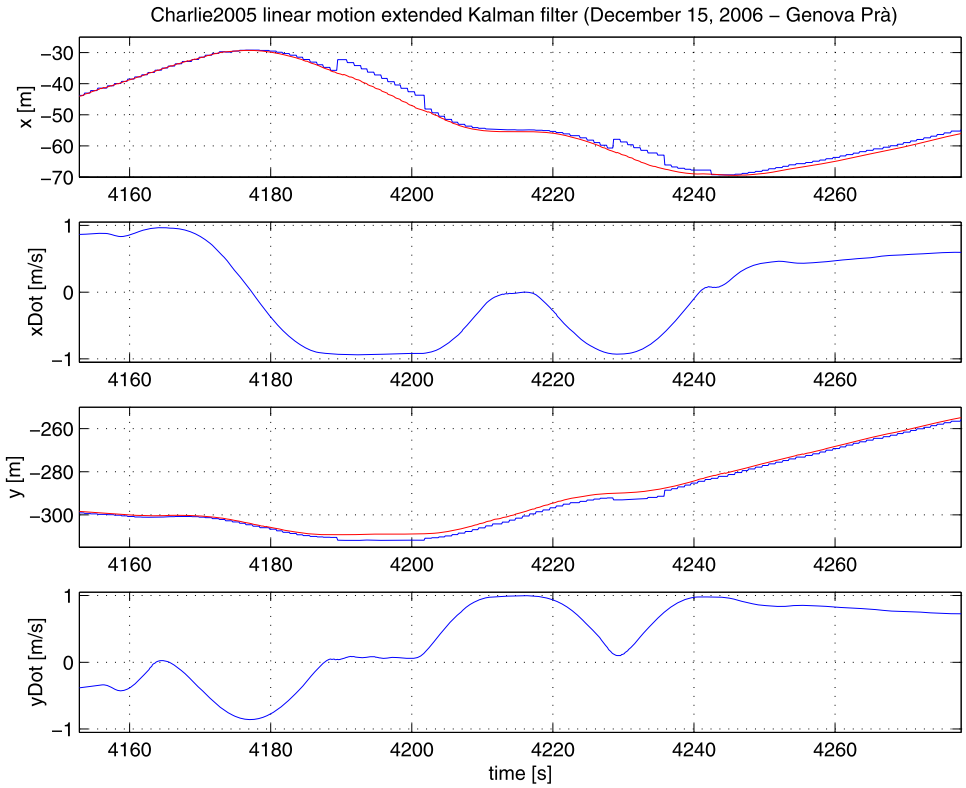

Fig. 8 (Color online) Linear motion estimation: extended Kalman filter + GPS discontinuities detection. From *top* to *bottom*: measured (*blue*) and estimated (*red*) x; estimated $\dot{x}$; measured (*blue*) and estimated (*red*) y; estimated $\dot{y}$

assuming $\sigma = 0.25$ for both the controllers and $\omega_n = 0.0125$ and $\omega_n = 0.025$ for the surge and yaw controller respectively.

Figure 10 shows the behaviour of the surge controller for a variety of reference speeds in presence of yaw manoeuvres. In particular, during the examined trial, the vehicle worked in auto-heading mode executing a number of left turns as pointed out by the relatively long time periods where a negative rudder angle δ is applied. The surge speed in the earth-fixed reference frame was controlled. Small displacements from the desired values are present basically in correspondence of vehicle yaw manoeuvrers, i.e. variations in the rudder-induced drag and sea current disturbance on the surge direction.

The behaviour of the yaw rate controller is shown in Fig. 11: steady-state precision is of the order of 1 deg/s and the rudder activity is quite smooth.

8.3 Guidance

The vehicle heading has been controlled with a PI-type guidance law (18) where $g_P = 0.5$ and $g_I = 0.025$ with hysteresis values for enabling/disabling the integrator equal to 5 deg and 10 deg respectively. As shown in Fig. 12, the steady-state precision of the resulting controller is higher than 1 deg with a quite smooth rudder activity.

As far as line-following is concerned, considering the approximative East-West orientation of the harbour channel were trials have been performed, the vessel has been commanded to follow lines parallel to the y axis. The guidance law (25) has been implemented with $g_P = 0.04\frac{180}{\pi}$ and $g_D = 0.4\frac{180}{\pi}$, while $\bar{b}$ has been chosen such that the approach angle $\bar{\beta} = a\sin(\bar{b})$ be equal to 60 deg in absence of sea current.

In the example shown in Figs. 13 and 14 the vessel was required to navigate alternatively Eastward, i.e. $\psi_L^* = 90$ deg, with x equal to -30 m and Westward changing its x coordinate to -40 m:

$$l^* = \left[x^*, \psi_L^*\right]: \begin{cases} \left[-30\text{ m},\ 90\text{ deg}\right] & t \le T1 \\ \left[-40\text{ m},\ -90\text{ deg}\right] & T1 < t \le T2 \\ \left[-30\text{ m},\ 90\text{ deg}\right] & T2 < t \le T3 \\ \left[-40\text{ m},\ -90\text{ deg}\right] & T3 < t \le T4 \\ \left[-30\text{ m},\ =90\text{ deg}\right] & t > T4 \end{cases} \quad (31)$$

The reference surge speed changed during the experiment as it follows:

$$u^* =: \begin{cases} 1.0\ \frac{\text{m}}{\text{s}} & t \le t1 \\ 1.2\ \frac{\text{m}}{\text{s}} & t1 < t \le t2 \\ 0.8\ \frac{\text{m}}{\text{s}} & t > t2 \end{cases} \quad (32)$$

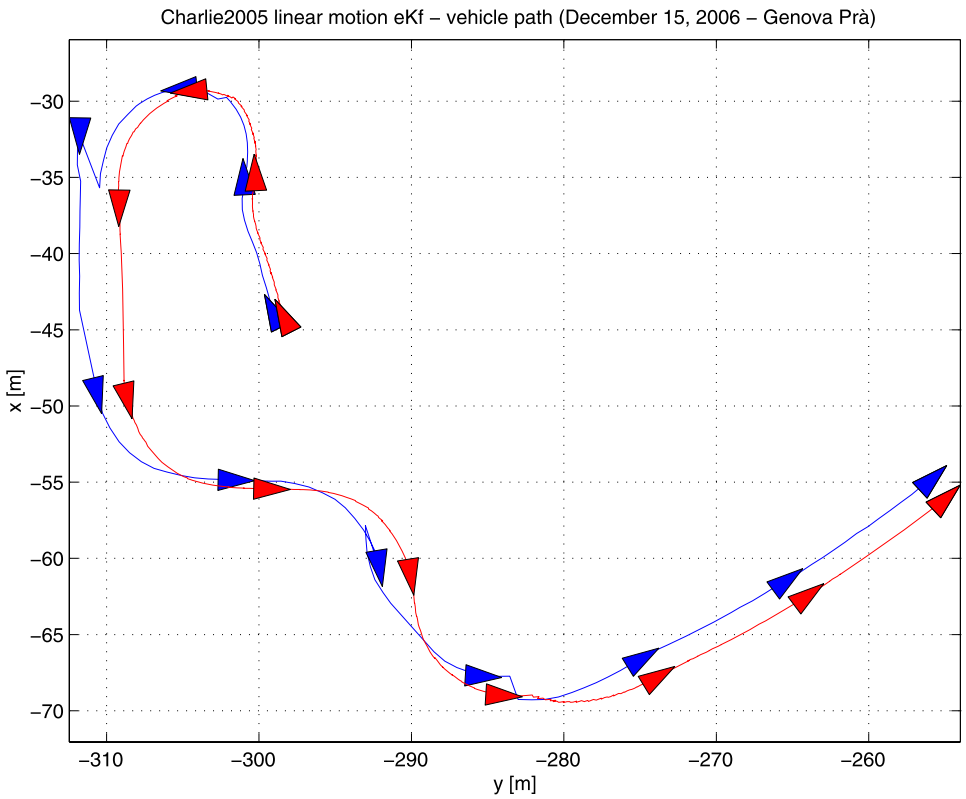

Fig. 9 (Color online) Linear motion estimation: extended Kalman filter + GPS discontinuities detection: measured (*blue*) and estimated (*red*) vehicle path

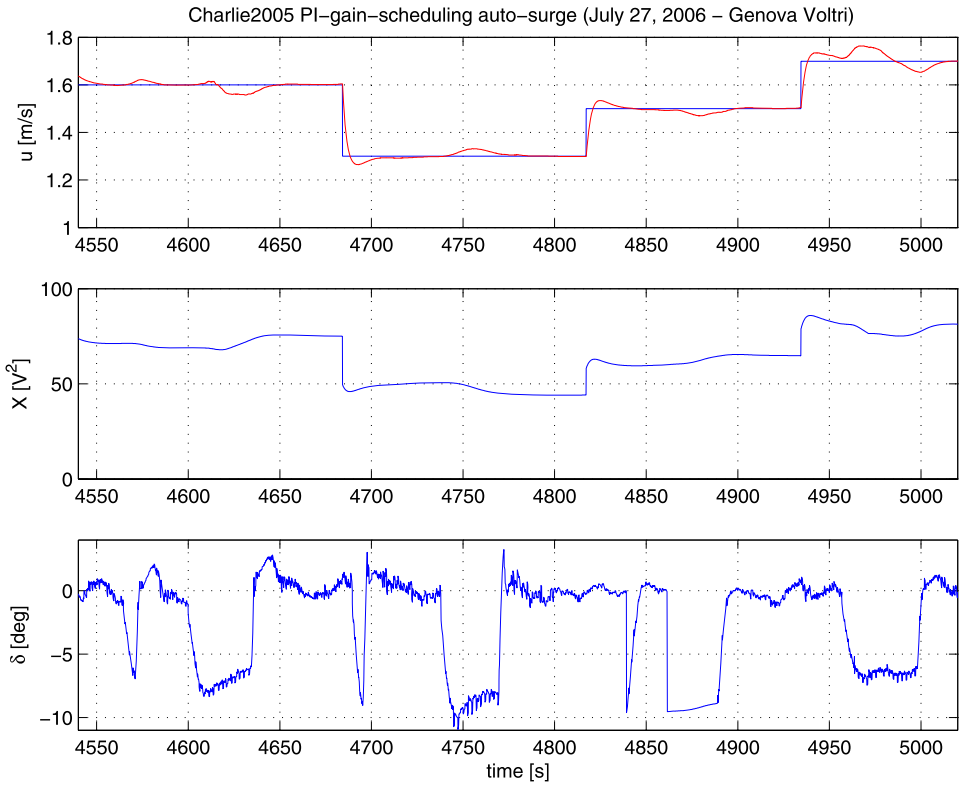

Fig. 10 (Color online) PI gain-scheduling surge control. From *top* to *bottom*: reference (*blue*) and estimated (*red*) surge; control force; commanded rudder angle

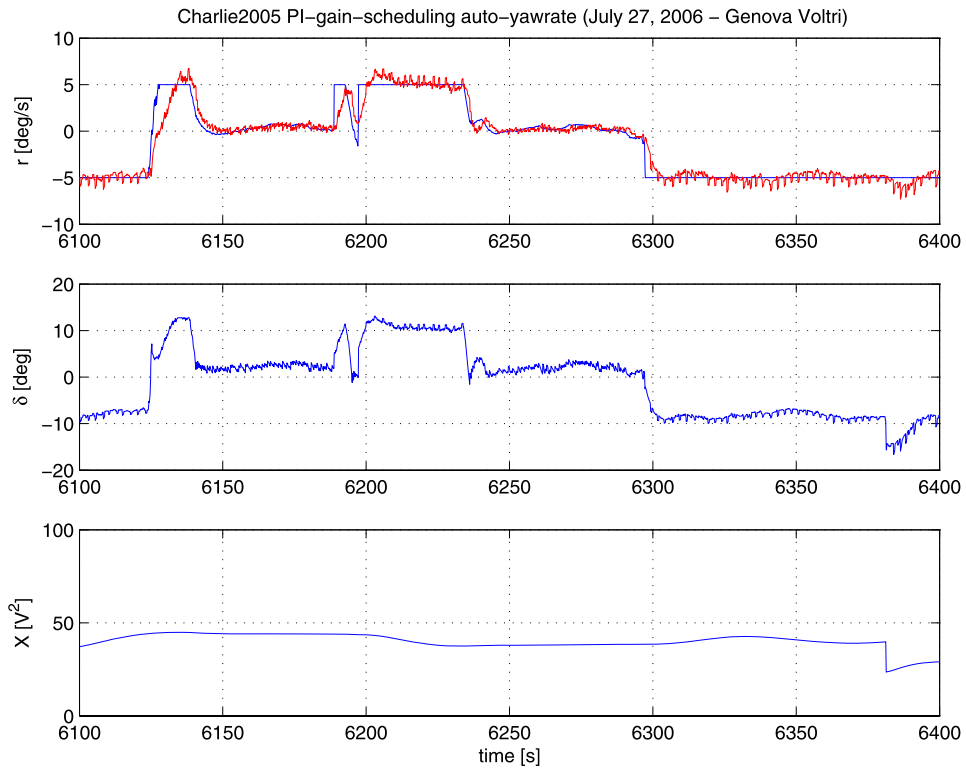

Fig. 11 (Color online) PI gain-scheduling yaw rate control. From *top* to *bottom*: reference (*blue*) and estimated (*red*) yaw rate; commanded rudder angle; applied surge force

As shown in Figs. 13 and 15, where the range d from the desired straight line is plotted, the line was correctly tracked with smooth heading variations and rudder action. It is worth noting how the proposed PD guidance law naturally steers the vehicle in order to compensate external disturbance: indeed, the vessel's heading stabilises around +86 deg while

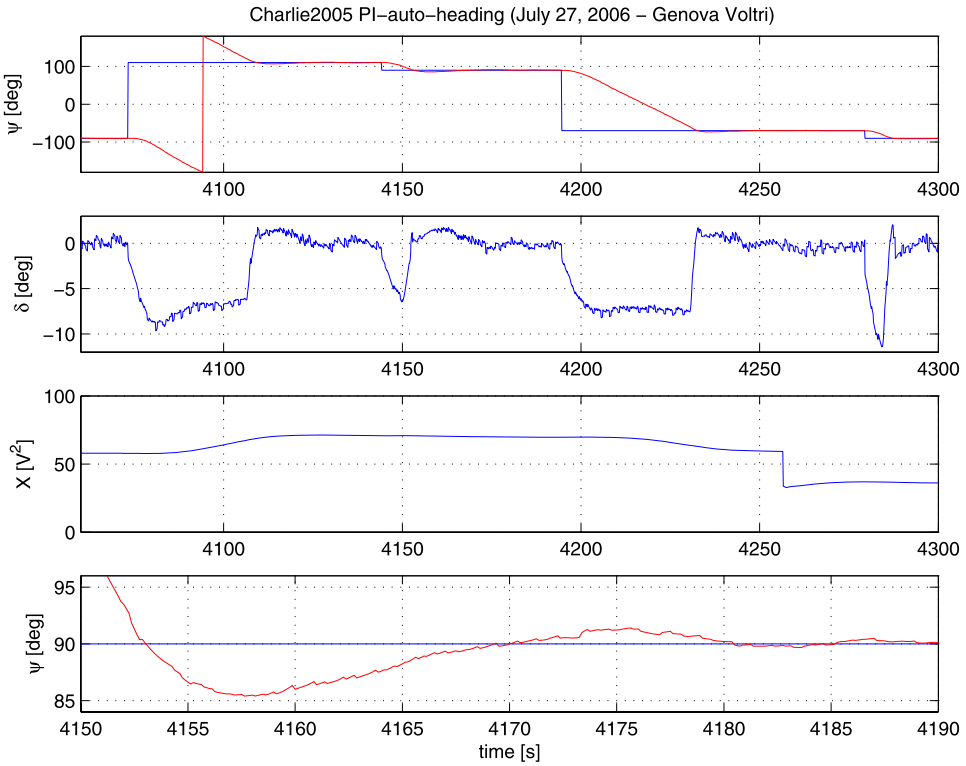

Fig. 12 (Color online) PI heading control. From *top* to *bottom*: reference (*blue*) and estimated (*red*) heading; commanded rudder angle; applied surge force; particular of reference (*blue*) and estimated (*red*) heading

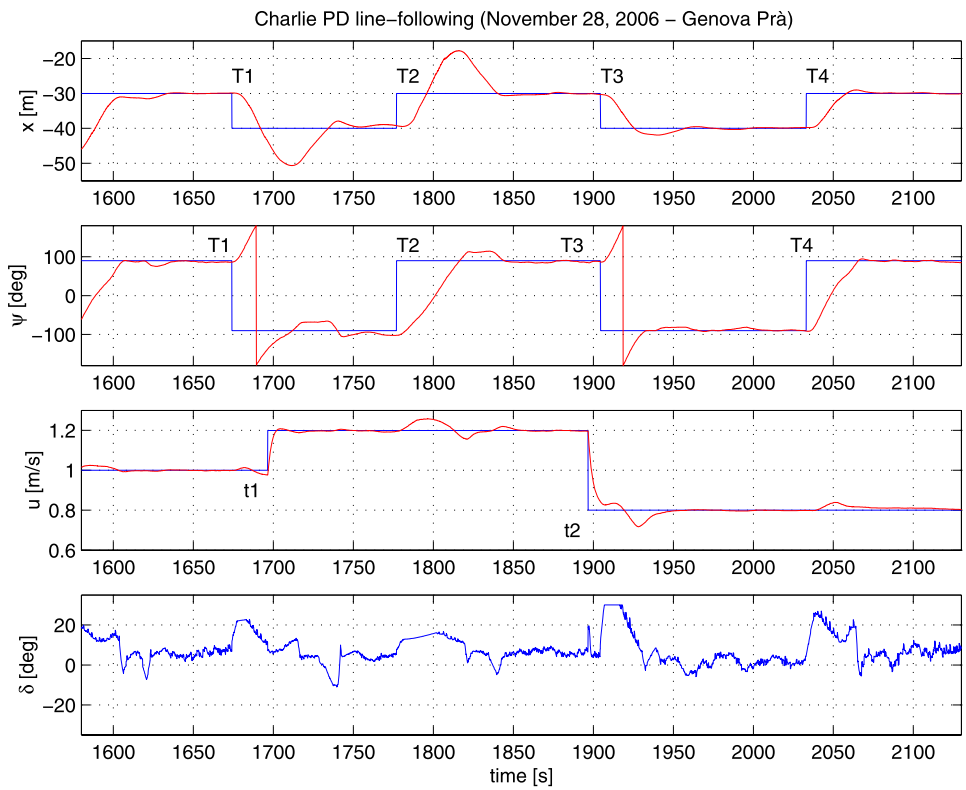

Fig. 13 (Color online) Line-following PD guidance (parallel to y-axis). From *top* to *bottom*: reference (*blue*) and estimated (*red*) x; reference line orientation (*blue*) and estimated heading (*red*); reference (*blue*) and estimated (*red*) surge; reference rudder angle

moving Eastward, being $\beta \simeq 4$ deg the orientation displacement required to compensate the combined effect of sea current and quite strong wind disturbances.

As shown in Fig. 14, due to the saturation of the requested yaw rate at 5 deg/s, the vehicle executed large U-turns, whose radius increased with the surge speed, while

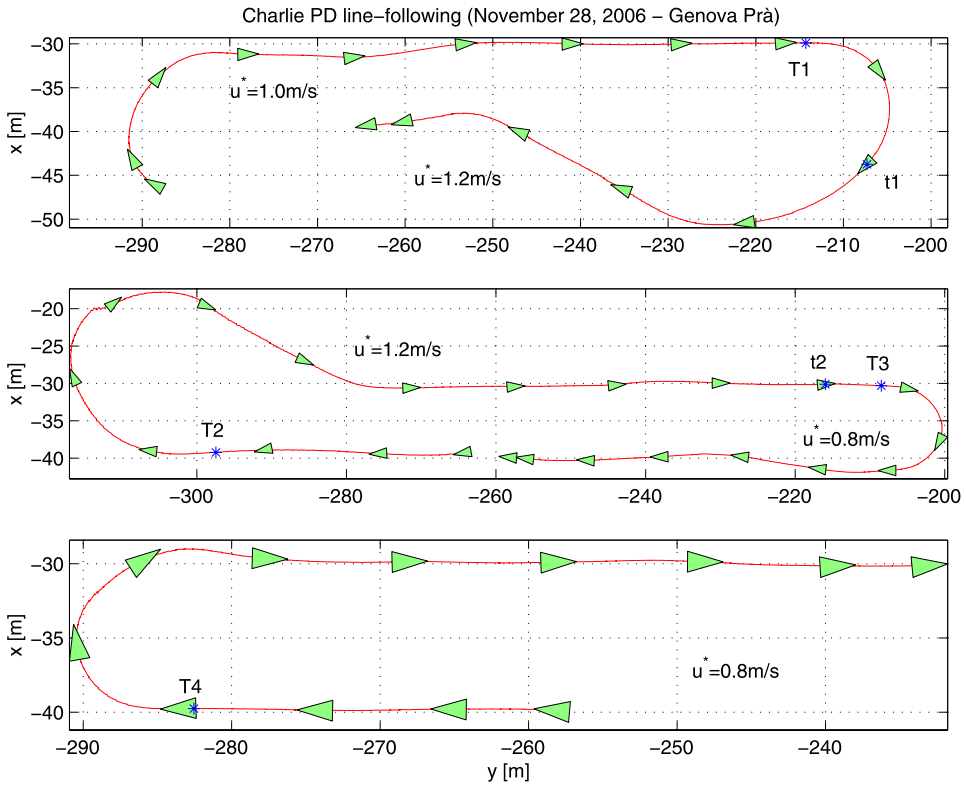

Fig. 14 (Color online) Line-following PD guidance (parallel to y-axis): vehicle path in the time intervals [1580, 1750] s, [1750, 2000] s and [2000, 2130] s (from top to bottom)

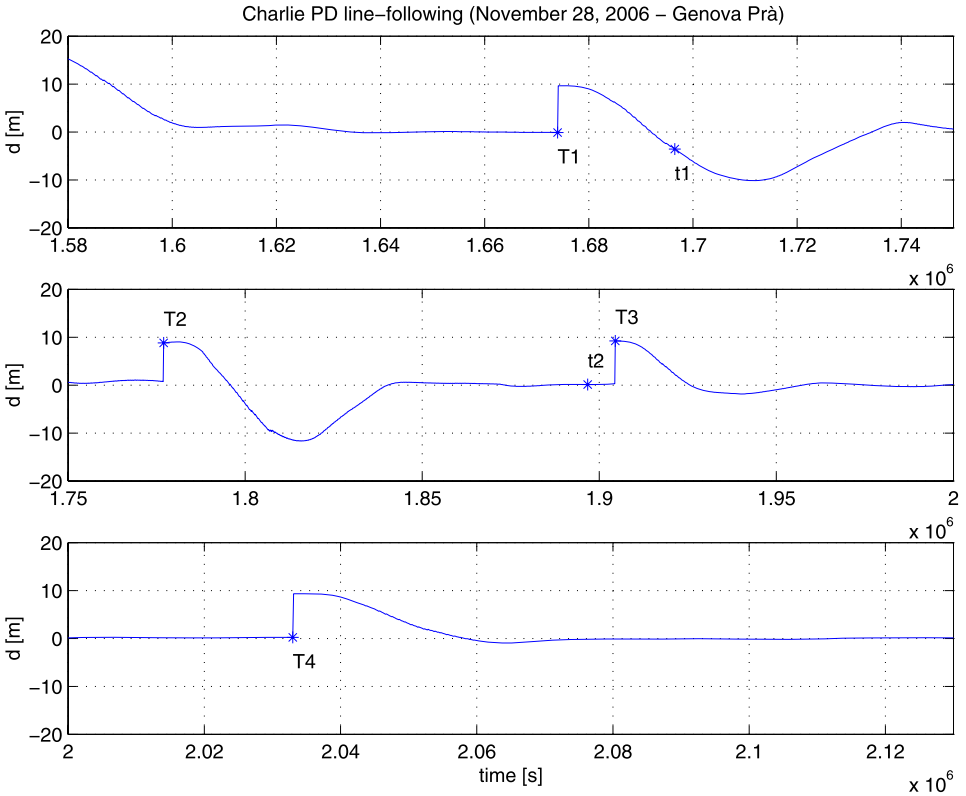

Fig. 15 (Color online) Line-following PD guidance (parallel to y-axis): range error d in the time intervals [1580, 1750] s, [1750, 2000] s and [2000, 2130] s (from *top* to *bottom*)

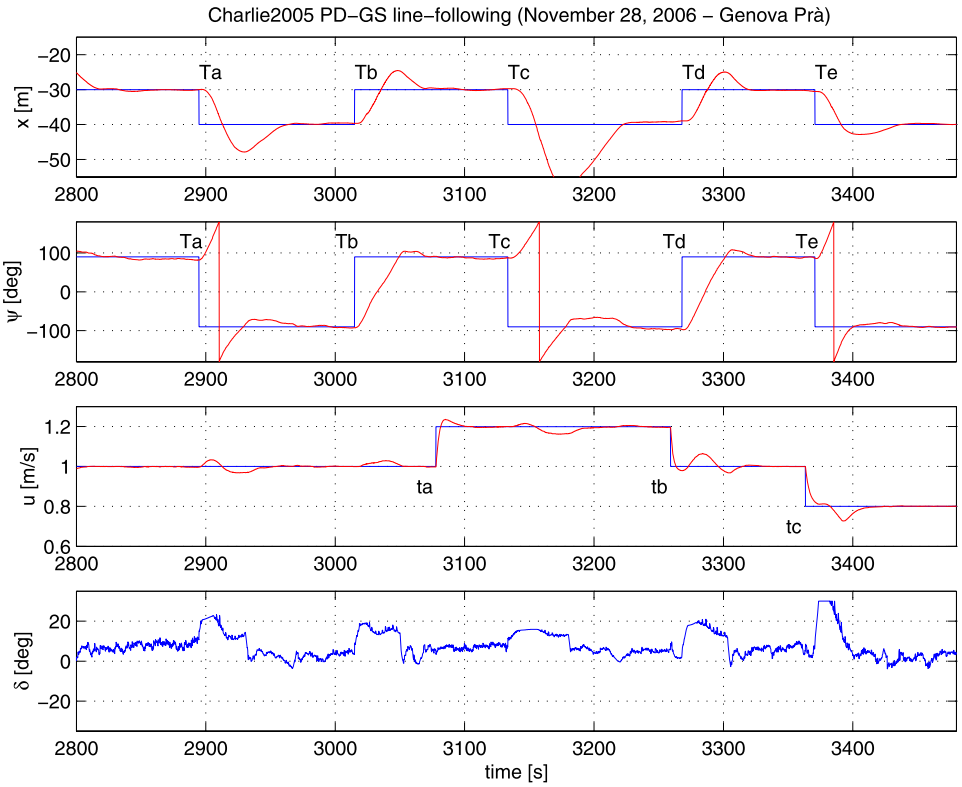

Fig. 16 (Color online) Line-following PD gain-scheduling guidance (parallel to y-axis). From top to bottom: reference (*blue*) and estimated (*red*) x; reference line orientation (*blue*) and estimated heading (*red*); reference (*blue*) and estimated (*red*) surge; reference rudder angle

approaching the desired straight line. On the basis of these results, the practical need of reducing the vehicle speed, while it is aligning with the desired direction of approach to the target line, in order to increase the manoeuvring efficiency has been heuristically addressed in Bibuli et al. (2007) in a generic path-following framework.

Experiments of PD line-following with a gain-scheduled choice of the gains g_P and g_D according to 30, with $\sigma_{LF} = 0.2$ and $\omega_{LF} = 0.02$, due to the limited variations in the vehicle surge speed, present similar results as shown in Figs. 16 and 17. In this case too, the vessel was required to navigate alternatively Eastward, i.e. $\psi_L^* = 90$ deg, with x equal to -30 m and Westward changing its x coordinate to -40 m:

$$l^* = \left[x^*, \psi_L^*\right]: \begin{cases} \left[-30\text{ m},\ 90\text{ deg}\right] & t \le Ta \\ \left[-40\text{ m},\ -90\text{ deg}\right] & Ta < t \le Tb \\ \left[-30\text{ m},\ 90\text{ deg}\right] & Tb < t \le Tc \\ \left[-40\text{ m},\ -90\text{ deg}\right] & Tc < t \le Td \\ \left[-30\text{ m},\ 90\text{ deg}\right] & Td < t \le Te \\ \left[-40\text{ m},\ =90\text{ deg}\right] & t > Te \end{cases} \tag{33}$$

while the reference surge speed changed during the experiment as it follows:

$$u^* =: \begin{cases} 1.0\ \frac{\text{m}}{\text{s}} & t \le ta \\ 1.2\ \frac{\text{m}}{\text{s}} & ta < t \le tb \\ 1.0\ \frac{\text{m}}{\text{s}} & tb < t \le tc \\ 0.8\ \frac{\text{m}}{\text{s}} & t > tc \end{cases} \tag{34}$$

9 Conclusions

The basic motion estimation, guidance and control system of the Charlie USV, an autonomous catamaran prototype equipped with a navigation package constituted only by GPS and compass, has been presented and discussed on the basis of experimental results. Simple conventional guidance and control laws, as well as motion estimation algorithms, allow the achievement of high precision performances in auto-heading and line-following, giving the possibility of demonstrating and exploiting a marine robotic vehicle within a short development time. Thus, research efforts, supported by experimental tests with a well-performing vehicle, will focus on the study, design and implementation of techniques for automatic obstacle detection and avoidance and advanced mission control, that, together with legal issues, represent, in the authors' opinion, the main bottlenecks in the development of common use unmanned surface vehicles. In addition, investigations will examine the issue of

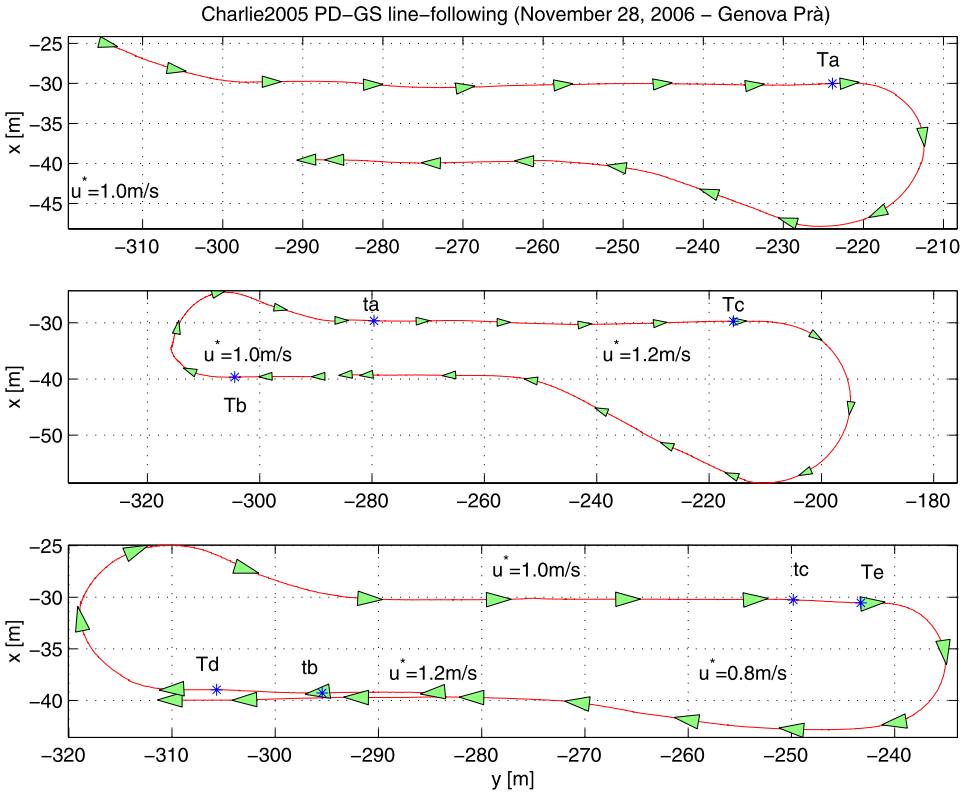

Fig. 17 (Color online) Line-following PD gain-scheduling guidance (parallel to y-axis): vehicle path in the time intervals [2800, 3000] s, [3000, 3250] s, and [3250, 3480] s (from *top* to *bottom*)

formally demonstrating the stability of the dual-loop scheme for managing system dynamics and kinematics, the design and implementation of globally stable path-following techniques embedding heuristics for increasing the manoeuvring efficiency in approaching the target.

Acknowledgements This work has been partially funded by PRAI-FESR Regione Liguria prot.5 "Coastal and harbour underwater anti-intrusion system".

The authors wish to thank Giorgio Bruzzone and Edoardo Spirandelli for their fundamental support in the development and operation of the Charlie USV and the Associazione Prà Viva for its kind help in allowing sea trials in the Genova Prà harbour.

References

Benjamin, M., & Curcio, J. (2004). COLREGS-based navigation in Unmanned Marine Vehicles. In *IEEE proceedings of AUV-2004*.

Bibuli, M., Caccia, M., & Lapierre, L. (2007). Path-following algorithms and experiments for an autonomous surface vehicle. In *Proc. of IFAC conference on control applications in marine systems.*

Breivik, M., & Fossen, T. (2004). Path following for marine surface vessels. In *Proc. of OTO'04* (pp. 2282–2289).

Bruzzone, G., & Caccia, M. (2005). GNU/Linux-based architecture for embedded real-time marine robotics control systems. In *Proc. of IARP int. workshop on underwater robotics* (pp. 137–144). Genova, Italy.

Caccia, M. (2006). Autonomous Surface Craft: prototypes and basic research issues. In *Proc. of IEEE 14th mediterranean conference on control and automation*.

Caccia, M. (2007). Vision-based ROV horizontal motion control: near-seafloor experimental results. *Control Engineering Practice*, *15*(6), 703–714.

Caccia, M., & Veruggio, G. (1999). Model-based heave motion estimation for variable configuration unmanned underwater vehicles. In *Proc. of IFAC world congress*.

Caccia, M., & Veruggio, G. (2000). Guidance and control of a reconfigurable unmanned underwater vehicle. *Control Engineering Practice*, *8*(1), 21–37.

Caccia, M., Bruzzone, G., & Veruggio, G. (2003). Bottom-following for remotely operated vehicles: algorithms and experiments. *Autonomous Robots*, *14*, 17–32.

Caccia, M., Bono, R., Bruzzone, G., Bruzzone, G., Spirandelli, E., Veruggio, G., Stortini, A., & Capodaglio, G. (2005). Sampling sea surface with SESAMO. *IEEE Robotics and Automation Magazine*, *12*(3), 95–105.

Caccia, M., Bruzzone, G., & Bono, R. (2006). Modelling and identification of the Charlie2005 ASC. In *Proc. of IEEE 14th mediterranean conference on control and automation*.

Cornfield, S., & Young, J. (2006). Unmanned surface vehicles—game changing technology for naval operations. In *Advances in unmanned marine vehicles. IEE control series* (pp. 311–328).

Curcio, J., Leonard, J., & Patrikalakis, A. (2005). SCOUT—A low cost autonomous surface platform for research in cooperative autonomy. In *Proc. of oceans 2005*.

Ebken, J., Bruch, M., & Lum, J. (2005). Applying UGV technologies to unmanned surface vessel's. In *SPIE proc. 5804, unmanned ground vehicle technology VII*.

Encarnaçao, P., & Pascoal, A. (2001). Combined trajectory tracking and path following: an application to the coordinated control of autonomous marine craft. *Proceedings of 40th IEEE Conference on Decision and Control*, *1*, 964–969.

Fryxell, D., Oliveira, P., Pascoal, A., Silvestre, C., & Kaminer, I. (1996). Navigation, guidance and control of AUVs: an application to the MARIUS vehicle. *Control Engineering Practice*, *4*(3), 401–409.

Gomes, P., Silvestre, C., Pascoal, A., & Cunha, R. (2006). A path-following controller for the DELFIMx autonomous surface craft. In *Proc. of 7th IFAC conference on manoeuvring and control of marine craft*. Lisbon: Portugal.

Khalil, H. (1996). *Nonlinear systems*. New York: Prentice Hall.

Lapierre, L., Soetanto, D., & Pascoal, A. (2003). Nonlinear path following with the applications to the control of autonomous underwater vehicles. In *Proc. of 42nd IEEE conference on decision and control* (pp. 1256–1261).

Majohr, J., & Buch, T. (2006). Modelling, simulation and control of an autonomous surface marine vehicle for surveying applications Measuring Dolphin MESSIN. In *Advances in unmanned marine vehicles. IEE Control Series* (pp. 329–352).

Manley, J. (1997). Development of the autonomous surface craft ACES. *Proceedings of Oceans'97 2*, 827–832.

Manley, J., Marsh, A., Cornforth, W., & Wiseman, C. (2000). Evolution of the autonomous surface craft AutoCat. *Proceedings of Oceans'00*, *1*, 403–408.

Martins, A., Almeida, J., Silva, E., & Pereira, F. (2006). Vision-based autonomous surface vehicle docking manoeuvre. In *Proc. of 7th IFAC conference on manoeuvring and control of marine craft*. Lisbon: Portugal.

Pascoal, A. et al. (2000). Robotic ocean vehicles for marine science applications: the European asimov project. In *Proc. of oceans 2000*.

Pascoal, A., Silvestre, C., & Oliveira, P. (2006). Vehicle and mission control of single and multiple autonomous marine robots. In *Advances in unmanned marine vehicles. IEE Control Series* (pp. 353–386).

Protector—Unmanned Naval Patrol Vehicle. http://www.israeli-weapons.com/weapons/naval/protector/Protector.html.

Ribeiro, M. (2004). *Kalman and extended Kalman filters: concept, derivation and properties* (Tech. Rep.). Institute for Systems and Robotics—Instituto Superior Tecnico, Lisbon.

Stingray—Unmanned Surface Vehicle (USV). http://www.defense-update.com/products/s/stingray.htm.

Xu, T., Chudley, J., & Sutton, R. (2006). Soft computing design of a multi-sensor data fusion system for an unmanned surface vehicle navigation. In *Proc. of 7th IFAC conference on manoeuvring and control of marine craft*.

Massimo Caccia graduated in the University of Genova in Electronics Engineering in 1991, joined CNR-IAN in 1993. His main research field is sensor-based motion estimation, guidance and control of unmanned marine vehicles. From 1998 to 2002 he was the main investigator in the research project "Marine robotics" of CNR-IAN, and then of the research group "Autonomous robotic systems and control" of CNR-ISSIA. In 2002-04 he was the principal investigator of the PNRA project "SEa Surface Autonomous MOdular unit (SESAMO)" for the sampling of sea surface microlayer with the Charlie USV in Antarctica, and currently coordinates the Regione Liguria PRAI-FESR project "Coastal and harbour underwater anti-intrusion system".

Marco Bibuli received the degree in information technology engineering at the Genova University in 2005. Since October 2005, he has a research grant at the Consiglio Nazionale delle Ricerche, Istituto di Studi sui Sistemi Intelligenti per l'Automazione (CNR-ISSIA). His research activity focuses on navigation, guidance and control of marine surface vehicles; mission control for mobile robots; and graphical human-machine interfaces (HMIs) for robotic system control and supervision. In 2007 he started PhD studies in Electronic, Robotics Information Technology and Telecommunication Engineering.

Riccardo Bono received his degree in Electronic Engineering in 1980 and in 1984 joined the CNR as research scientist. He operated in the field of Computer Generated Imagery, applied to training simulators. He was involved in research projects in the field of VTS and RVTS (acquisition and processing of maritime traffic data in the Mediterranean area during COST301 trials). He developes software architectures for control of unmanned marine vehicles and Human Computer Interfaces. He was Task Leader in EC MAST Projects AMADEUS 1 and 2 and ARAMIS. He participated to numerous Italian Expeditions to Antarctica, also as responsible of operating units for projects related to the Romeo ROV. In XVIII and XIX expeditions he was scientific responsible for the Technology sector.

Gabriele Bruzzone obtained his degree in electronic engineering at the Genoa University in 1993. He joined CNR as a research scientist in 1996. His research activity focuses on the study, design and development of real-time hardware and software control architectures and simulation of complex robotic systems, in particular manipulators and teleoperated underwater vehicles, and on the development of methodologies allowing access and availability to robotics resources via Internet. He contributed to the design and development of the ROVs Roby2 and Romeo. He was task leader in AC MAST Projects AMADEUS and ARAMIS. He was the person in charge of the e- Robot1 and e-Robot2 project experiments. In 2003–2004 he was the person in charge of the design, implementation and integration of the DACS of SESAMO project. Since 2005 he has been involved in the development of a software architecture for industrial automation and robotics applications based on free software.